IASS 2018 BOSTON, JULY 16-20
CREATIVITY IN STRUCTURAL DESIGN

Proceedings of the IASS Symposium 2018
Creativity in Structural Design
July 16-20, 2018, MIT, Boston, USA
Caitlin Mueller, Sigrid Adriaenssens (eds.)

Nonlinear growing caps

Paul M. SOBOTA[1], Keith A. SEFFEN[1*]

[1] Advanced Structures Group Laboratory, Department of Engineering, Cambridge University
Trumpington Street, Cambridge CB2 1PZ, UK
[*] kas14@cam.ac.uk

Abstract Engineers capture growth strains in two ways, reflecting the inherent bending-stretching nature of shells: by a strain gradient through the thickness or by an average in-plane value. We analyse their interaction by assuming a uniform displacement and growth-strain field in shells with elastic spring supports and a radial force applied to their outer boundary. The increased degree of statical indeterminancy enriches the variety of existing solutions and we distinguish two in-plane actuation modes which can induce Gaussian curvature via radially varying quadratic expansions in either the circumferential or radial direction. Using a Rayleigh-Ritz approach, we find closed-form solutions of the Föppl-von Kármán shell equations for the buckling thresholds, bistable limits and the post-buckled shape, which show good agreement with finite element reference solutions and available results from the literature. Moreover, we show that 'natural' growth modes, which evoke a change of shape without incurring elastic strain energy, can be achieved by employing quadratic radial expansions only. Additionally, we study unsupported shells subjected to higher-order actuation distributions, which give rise to natural growth modes with varying wavenumbers. Our approach dramatically simplifies an otherwise non-trivial general solution, and may be applied in novel generations of smart materials with actively tunable material properties.
Keywords: Actuation, growth, buckling, morphing structures, active control, adaptive structures, bistability, post-buckling, analytical solution

1. Introduction

The level of sophistication in floral systems in view of their shape-changing capabilities provides an inspiring variety of actuation methods for morphing structures. For example, growth strains within the plane of a simple leaf can result in its buckling into doubly-curved, non-Euclidean out-of-plane shapes, Fig. 1, which are stiffer and hence better at supporting self-weight compared to their planar counterparts. Conversely, differential growth strains through the thickness of certain 'solar-tracking' plants allow for their synchronised movement with the sun during the day. Such adaptive behaviour is often desired by Engineers to create multifunctional structures that can accommodate changing loading and environmental conditions; growth, in this sense, can be mimicked by using certain active materials, such as piezoelectric, shape memory alloys etc., which endow so-called inelastic or actuation strains without inducing stresses directly.

In this paper, we consider the shapes adopted by a linear elastic, circular plate subjected to particular growth strain variations. At any given point within the plate, the growth strain profile through the thickness is either linear or constant, giving rise to the respective descriptions of differential and uniform. The profile can also vary according to location within the plane of the plate.

Growth, or actuation, can thus stem from in-plane or out-of-plane actions, whose interaction gives rise to a variety of solutions. In particular, the buckling threshold can be precisely adjusted by combining both actuation modes, which can pave the way for compatible growth modes where large stress-free deformations occur [1]. These are known as *natural growth modes* and can be used for further structural modifications; for instance, transforming a flat disk into a stress-free doubly curved shell which also possesses an alternative stable state of equilibrium.

Figure 1: Non-Euclidean geometries in nature: (a) Elliptic example of *Euphorbia characias subspecies wulfenii* with approximately rotationally symmetric outer petals. (b,c) Hyperbolic examples: saddle-shaped petals of *Bergenia Ciliata* (b), and leaves of *Brachyglottis monroi* with higher wave number.

In this study, we focus on two novel aspects. First, we increase the degree of statical indeterminacy by supporting the shell boundary on linear elastic springs whilst maintaining a uniform Gaussian curvature growth field, g. The latter is an invariant property that distinguishes hyperbolic geometries ($g < 0$), from developable surfaces ($g = 0$) and elliptical shapes ($g > 0$). The supported edge, which is normally free, requires us to distinguish two different in-plane actuation methods that induce non-Euclidean geometries using a quadratic strain-field in either the radial *or* circumferential direction. These cause different boundary interactions, leading to richer solutions compared to unsupported cases from the literature. In addition, we enhance the interaction by imposing an extra uniform constant expansion term and a radial force applied to the shell edge. We then establish the condition for natural growth modes within all of these specifications.
Second, the recent development of novel manufacturing methods [2, 3] for 3D printing gels with tailored expansion coefficients, inspire us to study *unsupported* shells subjected to higher orders of actuation strain variations and thus non-uniform Gaussian curvatures. This gives rise to, in particular, hyperbolic periodically varying out-of-plane shapes.
Our analytical model in §2 assumes uniform curvature for the rotationally symmetric case which neglects the vanishing bending moment at the edge. We then compare our results to finite element (FE) reference solutions and present closed-form solutions of the Föppl-von Kármán (FvK) shell equations [4, 5] in §3; in addition, results for natural growth modes of radially varying negative Gaussian curvature are presented concomitant with a periodically varying deflection field in the circumferential direction.

2. Analytical Model

We distinguish three different configurations of an initially stress free disk of radius, a, and thickness, t, in the polar plane ($z = 0$) of a cylindrical coordinate system r, θ, z: the initial configuration, $\mathcal{B}_0$, a generally imaginary *target shape*, $\mathcal{B}_A$, without elastic resistance, and the resulting configuration, $\mathcal{B}$. The transition of a material point between these configurations is described by induced displacements due to actuation, $\boldsymbol{u}_A$, and elastic displacement, $\boldsymbol{u}_E$; their sum, $\boldsymbol{u}$, describes the transformation from $\mathcal{B}_0$ to $\mathcal{B}$. By employing FvK plate theory, we confine our findings to shallow gradients and small strains that consider, nonetheless, relatively large out-of-plane displacements, w, via mid-plane strains according to:

$$\varepsilon_r = \frac{\partial u_r}{\partial r} + \frac{1}{2}\left(\frac{\partial w}{\partial r}\right)^2 \;,\; \varepsilon_\theta = \frac{u_r}{r} + \frac{1}{r}\frac{\partial u_\theta}{\partial \theta} + \frac{1}{2}\left(\frac{\partial w}{r\,\partial \theta}\right)^2 \;,\; \varepsilon_{r\theta} = \frac{1}{2}\left(\frac{\partial u_r}{r\,\partial \theta} + \frac{\partial u_\theta}{\partial r} - \frac{u_\theta}{r} + \frac{\partial w}{r\,\partial \theta}\frac{\partial w}{\partial r}\right). \qquad (1)$$

The elastic in-plane response is described by an Airy stress function, Φ_E, which guarantees, by definition, in-plane equilibrium; it exists only for the elastic response, but not for the imposed strains of independent magnitude and direction.
We adopt Calladine's perspective [6] and understand shells as two different surfaces - one that solely bends, and another one that only stretches. Thus, it becomes apparent that the *incompatibility of actuation modes* in view of their Gaussian curvature, Δg_A, triggers an elastic reaction that enforces compatibility of the resulting shape via $g_B = g_S$, which is identical to the first FvK equation for isotropic materials. The incompatibility, $\Delta g_A = g_{BA} - g_{SA}$, is the difference of Gaussian curvature induced by bending actuation modes, g_{BA}, and in-plane actuation modes, g_{SA}. Because the intrinsic definition of Gaussian curvature is a linear partial differential equation,

$$g_S = \frac{1}{r}\left(\frac{\partial\,\varepsilon_r}{\partial r} - \frac{\partial^2\,(r\,\varepsilon_\theta)}{\partial r^2} - \frac{1}{r}\frac{\partial^2\,\varepsilon_r}{\partial\theta^2} + \frac{\partial}{\partial\theta}\left(\frac{\varepsilon_{r\theta}}{r}\right) + \frac{\partial^2\,\varepsilon_{r\theta}}{\partial r\partial\theta}\right), \tag{2}$$

we may calculate each contribution individually via $g_S = g_{SA} + g_{SE}$ using the same formula with corresponding substitutions; this does not, however, hold for its nonlinear extrinsic counterpart, $g_B = \kappa_r\kappa_\theta - \kappa_{r\theta}^2$, defined in curvatures, κ. We can therefore determine the elastic mid-plane response by rewriting the compatibility equation as

$$g_B - g_{SA} = g_{SE}\,, \tag{3}$$

where the left hand side can be considered as a *forcing term*. We make this expression amenable to a solution by employing a simple polynomial trial function for the elastic out-of-plane displacement. Since polynomials only approximate the equilibrium equations, we minimise the stored strain energy written as:

$$\begin{aligned}\Pi = \frac{1}{2}\int_0^a\int_0^{2\pi} &(m_r\kappa_{rE} + m_\theta\kappa_{\theta E} + m_{r\theta}\kappa_{r\theta E})\,r\,\mathrm{d}\theta\,\mathrm{d}r \\ &+ \frac{t}{2}\int_0^a\int_0^{2\pi}(\sigma_r\varepsilon_{rE} + \sigma_\theta\varepsilon_{\theta E} + \sigma_{r\theta}\varepsilon_{r\theta E})\,r\,\mathrm{d}\theta\,\mathrm{d}r \;+\; a\int_0^{2\pi}\left(\frac{K_u u_r^2}{2} - n_r u_r\right)\Big|_{\rho=1}\mathrm{d}\theta\,.\end{aligned} \tag{4}$$

The first and second terms are the bending- and stretching energies, respectively; at the edge where $\rho = 1$, K_u represents the stiffness of a radial spring whilst n_r describes a radial force per unit circumference. These two features introduce additional complexity to the solutions by triggering an elastic reaction without need of the forcing term in Eqn (3). Our assessment of natural growth modes is now performed for the rotationally symmetric case.

2.1. Growth modes of constant g: rotationally symmetric deflections

Positive values of g lead to elliptic geometries that engender symmetric deformations. The nonlinear strain definition in Eqn (1) simplifies to:

$$\varepsilon_r = \frac{\partial u_r}{\partial r} + \frac{1}{2}\left(\frac{\partial w}{\partial r}\right)^2 \quad , \quad \varepsilon_\theta = \frac{u_r}{r} \quad , \quad \varepsilon_{r\theta} = 0\,. \tag{5}$$

In a Rayleigh-Ritz approach, we assume the nonlinear elastic deflection term to be: $w_E = \eta_E\,(1-\rho^2)$, where $\rho = r/a$ is the dimensionless radius and η_E is a degree of freedom equivalent to the midpoint deflection. This shape is similar to the out-of-plane actuation mode, $w_A = \eta_A\,(1-\rho^2)$, and the total deflection reads $w = w_E + w_A$. The deliberate choice of w_E drastically simplifies the problem by enabling uniform curvatures,

$$\kappa_r = \frac{\partial^2 w}{\partial r^2} = \frac{2}{a^2}\,(\eta_E + \eta_A) \quad , \quad \kappa_\theta = \frac{1}{r}\frac{\partial w}{\partial r} = \frac{2}{a^2}\,(\eta_E + \eta_A) \quad \text{and} \quad \kappa_{r\theta} = 0\,. \tag{6}$$

These, however, neglect the boundary condition of a vanishing bending moment at the edge; but it can be shown that the equilibrium condition is satisfied on average across the shell, and in return we obtain closed form expressions for the buckling threshold and the post-buckled geometry.
For in-plane actuation, we consider a nonlinear inelastic strain distribution that resembles commonly encountered but simplified growth patterns in Nature:

$$\varepsilon_{rA} = \hat{\epsilon}_r \rho^2 + \hat{\epsilon}_0 \quad , \quad \varepsilon_{\theta A} = \hat{\epsilon}_\theta \rho^2 + \hat{\epsilon}_0 \quad \text{and} \quad \varepsilon_{r\theta A} = 0\,. \tag{7}$$

The first two strain-parameters $\hat{\epsilon}_r$ and $\hat{\epsilon}_\theta$ describe an orthotropic growth process with a quadratic radial variation, and $\hat{\epsilon}_0$ denotes an isotropic growth strain similar to uniform thermal expansion; according to Eqn (2), their corresponding Gaussian curvature reads: $g_{SA} = 2(\hat{\epsilon}_r - 3\hat{\epsilon}_\theta)/a^2$. By substituting the strain expressions in Eqn (2) with equivalent stresses before using $\sigma_r = 1/r \cdot \partial\, \Phi_E/\partial r$ and $\sigma_\theta = \partial^2\Phi_E/\partial r^2$, we can rewrite:

$$g_B - g_{SA} = -\frac{1}{E}\left(\frac{\mathrm{d}^4\Phi_E}{\mathrm{d}r^4} + \frac{2}{r}\frac{\mathrm{d}^3\Phi_E}{\mathrm{d}r^3} - \frac{1}{r^2}\frac{\mathrm{d}^2\Phi_E}{\mathrm{d}r^2} + \frac{1}{r^3}\frac{\mathrm{d}\Phi_E}{\mathrm{d}r}\right), \tag{8}$$

where E denotes the Young's modulus. The solution of this differential equation,

$$\Phi_E = \frac{E\rho^4}{32}\left(a^2(\hat{\epsilon}_r - 3\hat{\epsilon}_\theta) - 2(\eta_E + \eta_A)^2\right) + C_1 r^2\,, \tag{9}$$

possesses a constant of integration that we use to satisfy the radial boundary condition in Fig. 2: in particular, we prescribe a compatible displacement u_r at $\rho = 1$ with an in-plane spring of stiffness, K_u, and an outwards pointing radial force per unit circumference, n_r, at the edge via

$$K_u u_r\,|_{\rho=1} = -t\,\sigma_r\,|_{\rho=1} + n_r\,. \tag{10}$$

After substituting the strain energy functional now only depends on η_E, with equilibrium configurations determined by $\partial\Pi/\partial\eta_E = 0$. Their stability depends on the sign of $\partial^2\Pi/\partial\eta_E^2$, which changes at the resulting buckling-thresholds, as discussed in §3 in terms of our actuation parameters as well as the boundary parameters.

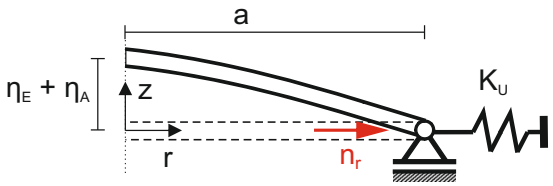

Figure 2: Rotationally symmetric spring supported boundary with radial force acting on the shell edge.

3. Results

We compare the results to finite element simulations conducted with the commercial software ABAQUS [7]. The quasi-static, implicit calculation uses a default time integration scheme with a free, quad-dominated mesh using over 1000 quadratic S8R elements for the disk, with $a = 1$, $t = 0.01$, $E = 10^7$, Poisson's ratio, $\nu = 0$, and a density of $2.58 \cdot 10^{-4}$. We prescribe a small imperfection with an amplitude of $t/1000$ consisting of the first ten eigenvalues, in order to seed out-of-plane buckling modes.

3.1. Rotationally symmetric shells

We now discuss the post-buckling behaviour of an initially stress-free disk emphasising the interaction of the in-plane actuation parameters $\hat{\epsilon}_r$, $\hat{\epsilon}_\theta$ and $\hat{\epsilon}_0$, in Eqn (7), the out-of-plane actuation parameter, η_A, Eqn (6), and additional boundary conditions, n_r and K_u, Eqn (10).

3.1.1. Buckling due to radial force and constant expansion ($\hat{\epsilon}_r = \hat{\epsilon}_\theta = \eta_A = 0 \rightarrow g_A = 0$)
Before we analyse cases with induced Gaussian curvature, g_A, we discuss the buckling thresholds of a radial force and a constant expansion to evaluate the suitability of our approach. From our stability criterion, $\partial^2\Pi/\partial\eta_E^2 = 0$, we have calculated the critical radial load as:

$$(n_r)_{cr} = \hat{\epsilon}_0\, K_u a - \frac{K_u t^2}{3a} - \frac{Et^3}{3a^2(1-\nu)}\,. \tag{11}$$

In the limiting cases of roller supports ($K_u = 0$) and pinned supports ($K_u \rightarrow \infty$), this simplifies to

$$(n_r)_{cr} = -\frac{Et^3}{3a^2(1-\nu)} \quad \text{or} \quad (\hat{\epsilon}_0)_{cr} = \frac{t^2}{3a^2}\,, \tag{12}$$

respectively. The uniform thermal expansion, $\hat{\epsilon}_0$, drops out in the first case since the imposed deformation is compatible ($g_A = 0$) and there is no support reaction in response to a radial displacement u_r; in the second case, the radial force does not affect the strain energy equation anymore since $u_r = 0$. For $\nu = 0$, the result of $n_{cr} = 3.33$ differs from the finite element result of $n_{cr} = 2.85$ by 16 % and provides a competitive accuracy compared to 'exact' approaches using Bessel functions Najafizadeh and Eslami [8] where n_{cr} is found to be 3.5. After buckling, the midpoint deflection becomes

$$\eta_E = \pm 2a\sqrt{-3\,\frac{n_r - (n_r)_{cr}}{Et + K_u a(7-\nu)}} \quad \text{with} \quad \lim_{K_u\rightarrow\infty}\eta_E = \pm 2a\sqrt{3\,\frac{\hat{\epsilon}_0 - (\hat{\epsilon}_0)_{cr}}{7-\nu}}\,, \tag{13}$$

Note that since n_r is negative and has a larger magnitude than $(n_r)_{cr}$, the square root term is positive. These structures are also bistable after buckling, because we can invert them to form its mirrored shape; each shape is separated by an energy barrier commensurate with snap-through buckling.

3.1.2. Buckling due to in-plane actuation ($\eta_A = 0$)
In a more general case, we consider additional in-plane actuations, which impose a non-Euclidean metric of $g_{SA} = 2(\hat{\epsilon}_r - 3\hat{\epsilon}_\theta)/a^2$. Using the previous solution, we find a buckling threshold, g^*_{SA} at which out-of-plane deformations begin:

$$g^*_{SA} = \frac{16}{a^4}\,\frac{Et^3/(1-\nu) + t^2 K_u a - 3K_u a^3(\hat{\epsilon}_\theta + \hat{\epsilon}_0) + 3n_r a^2}{Et + K_u a(7-\nu)}\,, \tag{14}$$

which simplifies to

$$g^*_{SA} = \frac{16}{a^2}\left[\frac{t^2}{a^2(1-\nu)} + \frac{3n_r}{\mathrm{E}t}\right] \quad \text{for } K_u = 0 \quad \text{and} \quad g^*_{SA} = \frac{16}{a^2}\,\frac{t^2 - 3a^2(\hat{\epsilon}_\theta + \hat{\epsilon}_0)}{a^2(7-\nu)} \quad \text{for } K_u \rightarrow \infty\,. \tag{15}$$

The corresponding post-buckled midpoint deflection takes a particularly compact form of

$$\eta_E = \pm\frac{a^2}{2}\sqrt{g_{SA} - g^*_{SA}}\,, \tag{16}$$

where the ± sign indicates a bistable response in either the up or down direction. For the simple case of $K_u = n_r = \hat{\epsilon}_0 = \hat{\epsilon}_\theta = 0$, we obtain a buckling limit of $g^*_{SA} = 16t^2/(1-\nu)a^4$ and a post buckled shape that is identical to the results of [1]. For other values of K_u, the shape differs only by the buckling threshold, g^*_{SA} in Eqn (14). The predictions for the midpoint deflection are compared to finite element results in Fig. 3 for $K_u \rightarrow \infty$ and, interestingly, they show an excellent agreement far beyond the limits of shallow shell theory, up to a value of $50t$, equal to one half of the shell planform radius.

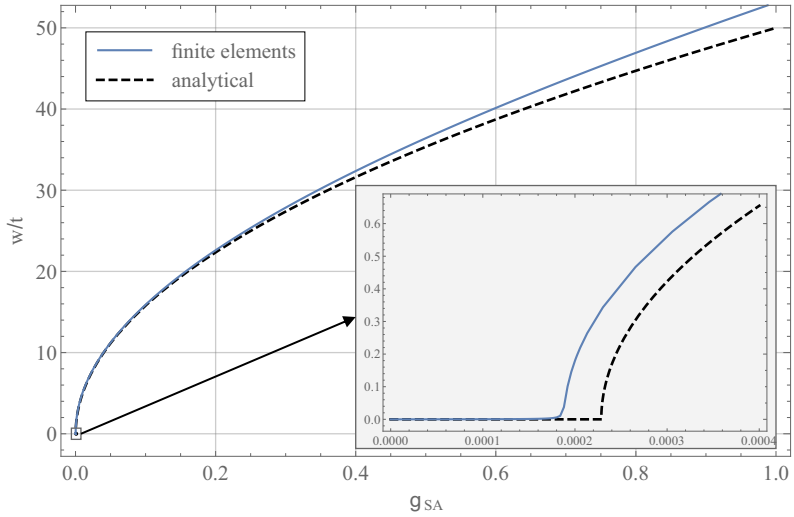

Figure 3: Disk subjected to a radially quadratically varying temperature field with $\hat{\epsilon}_r = \hat{\epsilon}_\theta = -\hat{\epsilon}_0$: FE results (full line) with $a/t = 100$ compared to analytical model (dashed line). The results are in excellent agreement with up to $w = 50t$. The inset-figure shows the buckling threshold in close-up.

3.1.3. Natural growth modes

By combining both actuation methods, it is possible to have 'deformed', stress-free non-Euclidean shapes. One way to determine the required parameters is to declare $\hat{\epsilon}_r$ and $\hat{\epsilon}_\theta$ as additional degrees of freedom, and to minimize the energy by ensuring that all eigenvalues of the stiffness matrix are positive. More intuitively, we may equate the in-plane stresses, σ_r and σ_θ, to zero, which provides two required equations to determine $\hat{\epsilon}_r$ and $\hat{\epsilon}_\theta$. The coincident results impose a Gaussian curvature $g_{BA} = g_{SA} = 4\eta_A^2/a^4$ without elastic components ($\eta_E = 0$) and

$$\hat{\epsilon}_r = \frac{2\eta_A^2}{a^2} + \frac{3n_r}{K_u a} - 3\hat{\epsilon}_0 \quad \text{and} \quad \hat{\epsilon}_\theta = \frac{n_r}{K_u a} - \hat{\epsilon}_0\,, \tag{17}$$

with a resulting radial edge displacement of $u_r = n_r/K_u$. Thus, natural growth modes are possible for the roller supported case with $n_r = 0$ or a sufficiently large spring stiffness to ensure a small u_r. In particular, the natural growth modes of Eqn (16) can be achieved by using radially quadratic variations of the actuated strain only via $\varepsilon_{rA} = 2(\rho\,\eta_A/a)^2$ and $\varepsilon_{\theta A} = 0$, when other influencing factors are absent ($n_r = \hat{\epsilon}_0 = 0$).

For corresponding bistability, the out-of-plane actuation modes need to be set to $\eta_A^2 \geq 16t^2/(1-\nu)$ for roller supported shells and to $\eta_A^2 \geq 16t^2(1-\nu)/(7-\nu)$ for pinned shells, respectively; for details about these thresholds, see [9].

3.2. Higher order natural growth modes without rotational symmetry

Relaxing rotational symmetry offers an interesting variety of achievable hyperbolic geometries. In contrast to elliptic geometries ($g > 0$), the asymmetry of hyperbolic geometries ($g < 0$) leads to out-of-plane shapes described by periodic 'waves'. To facilitate this non-trivial problem, we consider only the case of free plates without boundary supports: moreover, we confine our analysis to polynomial growth patterns without circumferential variations of the form:

$$\varepsilon_{rA} = \varepsilon_{\theta A} = \hat{\varepsilon}\, r^m \tag{18}$$

which give a corresponding negative Gaussian curvature of $g_{SA} = -\hat{\epsilon}_r\, m^2\, r^{-2+m}/a^m$. The simplest example of constant negative Gaussian curvature is a saddle, which is described by $r^2\cos(2\theta)$ in polar

coordinates. A generalisation of this case, $w_A = \eta_A \rho^i \cos(j\theta)$ does not show variations of Gaussian curvature in circumferential direction for $j = \pm i$, for which it reads: $g_{BA} = -(i-1)^2 i^2 \eta_A^2 \rho^{2i-4}/a^4$. Thus, with $i = m/2 + 1$ or $m = 2(i-1)$ a compatible deflected shape is given by

$$w = \eta_A r^i \cdot \cos(i\theta)\,, \tag{19}$$

where i is an integer greater than one. A natural growth mode without elastic stresses comes from setting

$$\hat{\varepsilon} = \frac{(2+m)^2}{16}\frac{\eta_A^2}{a^2}\,, \tag{20}$$

which ensures that $g_{BA} = g_{SA}$. However, actuation modes with $\eta_A \neq 0$ complicate the manufacturing process due to their circumferential variations and hence, it appears tempting to control the wavenumber by solely using a rotationally symmetric in-plane actuation mode of $\varepsilon_{rA} = \varepsilon_{\theta A} = \hat{\varepsilon}\rho^m$. Finite element simulations in Fig. 4 confirmed that setting ε_{rA} and $\varepsilon_{\theta A}$ proportional to $\rho^{i/2+1}$ in very thin shells without stipulating out-of-plane actuation modes results in i waves due to a negligible bending contribution. As soon as the thickness increases, the wave number is reduced, and an analytical description of this problem is currently under investigation.

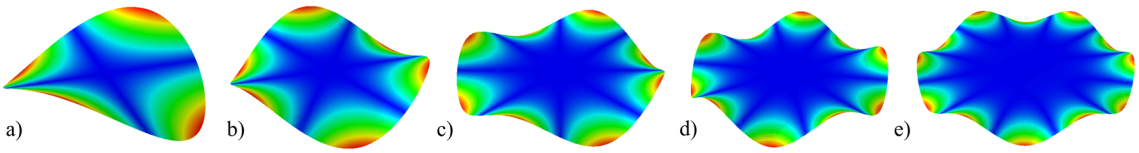

Figure 4: Magnitude of displacements according to FE results analysing the post-buckled shape for initially flat disks with $a/t = 1000$ subjected to grow strains proportional to ρ^2 (a), ρ^4 (b), ρ^6 (c), ρ^8 (d), and ρ^{10} (e). Increasing powers in the grow strain polynomial correlate with the wavenumber in the post-buckled shape via $\rho^{i/2+1}$ giving i waves.

4. Summary

This study has considered differential growth models in shallow shells that mimic simplified nonlinear growth patterns in Nature. In a first step, we employed a Rayleigh-Ritz approach assuming uniform curvature, to analyse various actuation methods and their corresponding buckling thresholds as well as post-buckling behaviour. In particular, we considered a three-parameter in-plane actuation mode, a uniform out-of-plane actuation mode, an additional radial force on the boundary as well as horizontal supports with variable stiffness. The results were found to be in good agreement with FE simulations and available literature results. The post-buckled shapes were found to be in excellent agreement, even far beyond the limits of shallow shell theory. When only in-plane actuation parameters were used, shells become bistable at the buckling threshold, since an energy barrier separates two possible shapes that show mirror symmetry with respect to the polar plane; however, these lose their symmetry as soon as out-of-plane growth modes are applied. By combining the first with the latter, we demonstrated that natural growth modes exist in the presence of horizontal supports, for which a single in-plane actuation parameter describing the quadratically varying radial grow strain suffices.
On hyperbolic shapes, we considered a centrally fixed shell, and demonstrated that certain natural growth modes can be used to actively control the wavenumber using in-plane actuation patterns without circumferential variations. This paper might inspire novel actuation methods in smart materials with actively tunable surface texture with application to problems, for example, on heat conductivity, adhesion, and light reflection.

References

[1] K. A. Seffen, C. Maurini, Growth and shape control of disks by bending and extension, Journal of the Mechanics and Physics of Solids 61 (2013) 190–204.
[2] Y. Klein, E. Efrati, E. Sharon, Shaping of elastic sheets by prescription of non-Euclidean metrics, Science 315 (2007) 1116–1120.
[3] A. S. Gladman, E. A. Matsumoto, R. G. Nuzzo, L. Mahadevan, J. A. Lewis, Biomimetic 4D printing, Nature Materials 15 (2016) 413.
[4] A. Föppl, Vorlesungen über Technische Mechanik, volume 5, BG Teubner, 1907.
[5] T. von Kármán, Festigkeitsprobleme im Maschinenbau, Encyclopädie der mathematischen Wissenschaften iv, 1910.
[6] C. R. Calladine, Theory of Shell Structures, Cambridge University Press, 1983.
[7] Hibbitt, Karlsson, Sorensen, ABAQUS/Standard User's Manual, Version 6.14, volume 1, Hibbitt, Karlsson & Sorensen, 2014.
[8] M. Najafizadeh, M. Eslami, Buckling analysis of circular plates of functionally graded materials under uniform radial compression, International Journal of Mechanical Sciences 44 (2002) 2479–2493.
[9] P. M. Sobota, K. A. Seffen, Effects of boundary conditions on bistable behaviour in axisymmetrical shallow shells, Proceedings of the Royal Society of London A 473 (2017) 20170230.